THE AMERICAN MINERALOGIST, VOL. 55, NOVEMBER-DECEMBER, 1970

EQUILIBRIUM RELATIONS OF HYPERSTHENE, PIGEONITE AND AUGITE IN CRYSTALLIZING MAGMAS: MICROPROBE STUDY OF A PIGEONITE ANDESITE FROM WEISELBERG, GERMANY

YASUO NAKAMURA AND IKUO KUSHIRO, *Geological Institute, University of Tokyo, Tokyo, Japan*

ABSTRACT

Compositional relations of five different coexisting pyroxenes, hypersthene, pigeonite and augite phenocrysts and ferropigeonite and ferroaugite of the groundmass in a pigeonite andesite from Weiselberg have been determined with the electron probe microanalyzer. It is shown that as fractional crystallization proceeded, the phenocryst pyroxene assemblage varied from hypersthene-augite of relatively low Fe/Mg ratio, through hypersthene-pigeonite-augite of varying Fe/Mg ratio, to pigeonite-augite of relatively high Fe/Mg ratio. Eight pairs of hypersthene-pigeonite of different Fe/Mg ratio were analyzed to determine the partition coefficient of Mg-Fe between these minerals. Groundmass ferropigeonite and ferroaugite represent the latest crystallized pyroxenes in this andesite. Neither subcalcic augite nor subcalcic ferroaugite crystallized at any stage of crystallization. It is suggested that changeover from hypersthene to pigeonite during the crystallization sequence is a result of the reaction hypersthene + liquid $\rightleftarrows$ pigeonite. The region where hypersthene, augite and pigeonite coexist shifts toward the iron-rich side of the quadrilateral with lowering temperature. This interpretation is different from that suggested previously and would be applicable to the hypersthene-pigeonite relations in many other igneous rocks.

INTRODUCTION

Many pyroxenes have been separated from various volcanic rocks and chemically analyzed; however, most of the analyses represent the bulk compositions of the zoned pyroxenes or mixtures of two or more coexisting pyroxenes because of the difficulty of separating fine-grained and zoned pyroxenes in volcanic rocks. The compositions of pyroxenes in volcanic rocks, particularly those in the groundmass, should be redetermined with the electron probe microanalyzer. In a previous paper (Nakamura and Kushiro, 1970), the compositional relations of the coexisting orthopyroxene, augite and pigeonite in a tholeiitic andesite from Hakone Volcano have been determined. To understand the hypersthene-pigeonite-augite relation in more detail, a pigeonite andesite from Weiselberg, Germany has been selected. The microprobe analysis was made carefully on hypersthene, pigeonite, and augite which are in contact or occur as contiguous crystals in both phenocryst and groundmass. On the basis of the present analytical data the crystallization course of pyroxenes in tholeiitic magma is discussed and a new interpretation of hypersthene-pigeonite relation is presented.

Description of Rock

The pigeonite andesite used for the present studies is the specimen studied by Kuno (1947 and 1955). It was originally described as 'weiselbergite' by Rosenbusch (1887). The rock analysis given by Tröger (1934) is as follows (wt. %): SiO_8 62.62, Al_2O_3 13.88, Fe_2O_3 2.18, FeO 4.36, MnO 0.20, MgO 1.48, CaO 4.31, Na_2O 4.65, K_2O 1.29, TiO_2 0.99, P_2O_5 0.07, CO_2 0.24, S 0.03, BaO 0.06, H_2O+3.58, H_2O-0.30. The normative pyroxene composition is Di Wo 2.7, En 3.8, Fs 5.2 (5.4, Hy 6.3) weight percent. Phenocryst minerals are plagioclase (labradorite-andesine), hypersthene, pigeonite, augite, Fe-Ti oxide (mostly ilmenite with oxidized rim) and apatite (inclusion in hypersthene phenocryst). Augite is rare and occurs as random growth inclusions in hypersthene and pigeonite phenocrysts and as rims to pigeonite phenocrysts. The grain size of the phenocrysts ranges from 0.1 to 1.0 mm. The groundmass consists of very fine-grained pigeonite-augite composite grains, andesine, altered Fe–Ti oxide, apatite and brown glass. The groundmass Fe–Ti oxide mineral is completely oxidized or hydrated. The brown glass includes very fine-grained crystals and similar to crystallite. Its composition, including the minute crystals, is rhyolitic as shown in the following section. The grain size of the groundmass minerals ranges up to 0.05 mm. The modal analysis is as follows:

Phenocrysts	(vol. %)	*Groundmass*	(vol. %)
plagioclase	7.5	plagioclase	15
hypersthene	0.3	augite }	8
pigeonite	2.2	pigeonite }	
augite	< 0.1	Fe–Ti oxide	2
Fe–Ti oxide (ilmenite)	0.6	apatite	< 0.5
apatite	< 0.1	glass	64
	11		89

Analytical Method

Analyses were made with a Japan Electron Optics Laboratory electron probe microanalyzer Model JXA-5, with a 40° take-off angle. The conditions of analysis, standard materials and correction procedures are as described previously (Nakamura and Kushiro, 1970; Kushiro and Nakamura, 1970). All corrections were calculated with a HITAC computer using a program provided by Dr. Mituko Ozima. The analysis of Na in pyroxene was made with a 0.04 μA specimen current, same as that for the analysis of the other elements; however, the standard albite was moved at 100 μm/min to avoid Na volatilization. The analysis of Na in plagioclase was made with a 0.02 μA specimen current and with a moving speed of 50 μm/min, and the analysis of glass was made with 0.01 μA specimen current and 20 μm electron beam-size. Counts of 5 spots were averaged for each analysis except for the analysis of very small grains such as inclusions of augite in hypersthene and some groundmass augite and pigeonite.

Results

Thirty-six complete analyses and sixteen partial analyses of various pyroxenes have been obtained. Selected analyses are shown in Table 1 and all are plotted on Ca–Mg–Fe diagrams (Figs. 1 and 2). Since most of the pyroxenes are more or less zoned, careful analysis was made to determine their compositional ranges and to determine the compositions of the different pyroxenes which are in direct contact. As shown in Figures 1 and 2, phenocryst Ca-poor pyroxenes are hypersthene-ferrohypersthene ($Ca_4Mg_{54}Fe_{42}$—$Ca_4Mg_{47}Fe_{49}$) and pigeonite-ferropigeonite ($Ca_8Mg_{48}Fe_{44}$—$Ca_9Mg_{35}Fe_{56}$), whereas phenocryst Ca-rich pyroxene is augite-ferroaugite ($Ca_{38}Mg_{37}Fe_{25}$—$Ca_{35}Mg_{29}Fe_{36}$). In the following pages, hypersthene-ferrohypersthene, pigeonite-ferropigeonite and augite-ferroaugite will be simply written as hypersthene, pigeonite, and augite, respectively. Phenocryst augite occurs as random growth inclusions in phenocryst hypersthene and pigeonite and at the margin of some pigeonite phenocrysts. Phenocryst hypersthene is always rimmed by pigeonite and is not in contact with glass, whereas phenocryst pigeonite is in contact with glass. Groundmass pyroxenes are pigeonite and augite of relatively high Fe/Mg ratios, both of which are in contact with glass.

The compositional zoning of phenocryst hypersthene and pigeonite is shown in Figure 3. It is always normal zoning: Fe/Mg ratio increases regularly from the core outward, as shown in Figure 4. Near the margin of the crystals, the Fe/Mg ratio increases rapidly, however, no discontinuous zoning was observed. Such regular and continuous zoning contrasts with the zoning of phenocryst and groundmass pyroxenes in the andesite of Hakone (Nakamura and Kushiro, 1970), which is not regular, and that in the andesite from Haruna volcano (Oshima, oral communication), which is reversed at the phenocryst margin. The Fe/Mg ratios of groundmass pigeonite are slightly higher than those of the phenocryst rims. Successive and continuous iron-enrichment from the core of phenocryst pigeonite to groundmass pigeonite suggests that there was no sudden great change of physical conditions between the stage of phenocryst crystallization and that of groundmass crystallization.

The compositional ranges of hypersthene and pigeonite overlap with respect to Fe/Mg, as shown in Figures 1, 2 and 3. The contiguous hypersthene, pigeonite and augite of grain No. 12 (Fig. 6A) have been analyzed to determine their compositional relations and to obtain the three-phase triangle. Compositions have been also determined for the contiguous crystals of hypersthene and pigeonite, hypersthene and augite, and pigeonite and augite, and their tie lines have been obtained

TABLE 1. SELECTED MICROPROBE ANALYSES OF PYROXENES

	Hypersthene					Pigeonite									Augite				
	Phenocryst					Phenocryst					Rim of Phenocryst			Groundmass		Phenocryst			Rim of Phenocryst	Ground-mass
Grain No.	4		12	69	74	4	12	26	63	69	4	26	68	103	108	12	63	74	68	103
Point of Analysis	4–3	4–4	12–4	69–2	74–4	4–2	12–6	26–2	63–2	69–1	4–1	26–1	68–4	103–2		12–5	63–3	74–3	68–3	103–1
SiO_2	51.2	51.1	51.6	50.6	50.6	50.8	51.1	50.8	50.1	50.7	50.4	49.6	50.3	49.4	49.4	50.3	50.2	49.4	50.8	49.9
Al_2O_3	0.70	0.84	0.67	0.70	0.80	0.61	0.62	0.60	0.56	0.59	0.57	0.48	0.53	0.76	0.63	1.43	1.39	1.48	0.72	0.73
TiO_2	0.34	0.44	0.33	0.37	0.40	0.28	0.29	0.28	0.27	0.29	0.28	0.29	0.27	0.39	0.48	0.68	0.54	0.64	0.50	0.48
FeO[a]	27.7	26.0	27.0	29.5	29.3	27.4	26.9	27.9	29.0	29.0	29.7	32.7	30.8	32.6	32.3	15.1	17.5	16.6	21.2	21.4
MnO	0.58	0.54	0.56	0.59	0.59	0.63	0.66	0.67	0.65	0.68	0.75	0.78	0.77	0.81	0.80	0.38	0.39	0.37	0.52	0.50
MgO	17.1	18.4	18.3	15.8	16.1	15.5	16.2	15.1	14.3	14.6	13.8	11.9	12.7	11.5	10.9	12.4	11.1	11.4	9.46	9.16
CaO	1.98	2.06	1.86	1.91	1.93	3.99	4.07	4.36	4.08	3.93	3.86	3.77	3.77	4.00	4.29	18.1	17.6	18.1	15.9	16.2
Na_2O	0.04	0.05	n.d.	0.04	0.05	0.09	n.d.	0.08	0.08	0.09	0.05	0.09	0.07	0.06	0.07	n.d.	0.24	0.25	0.27	0.21
Total	99.6	99.4	100.3	99.5	99.8	99.3	99.8	99.8	99.0	99.9	99.4	99.6	99.2	99.5	98.9	98.4	99.0	98.2	99.4	98.6
Z	2.00	2.00	2.00	2.00	2.00	2.00	2.00	2.00	2.00	2.00	2.00	2.00	2.00	2.00	2.00	2.00	2.00	2.00	2.00	2.00
WXY	1.99	2.01	2.00	2.00	2.00	2.00	2.00	2.00	2.01	2.00	2.00	2.00	1.99	2.00	1.99	2.00	2.01	2.02	1.99	2.00
Ca	4.2	4.3	3.9	4.1	4.1	8.5	8.6	9.3	8.8	8.4	8.3	8.2	8.3	8.8	9.6	38.3	37.7	38.6	34.9	35.4
Mg	50.2	53.4	52.6	46.8	47.4	46.0	47.4	44.5	42.7	43.3	41.5	36.0	38.9	35.1	33.9	36.7	33.1	33.8	28.9	27.9
Fe	45.6	42.3	43.6	49.1	48.5	45.5	44.1	46.2	48.5	48.3	50.2	55.7	52.8	56.1	56.5	25.0	29.2	27.7	36.2	36.6
Contiguous phase analyzed	Pig. 4–2		Aug. 12–5 Pig. 12–6	Pig. 69–1	Aug. 74–3	Hyp. 4–3	Hyp. 12–4 Aug. 12–5		Aug. 63–3	Hyp. 69–2			Aug. 68–3	Aug. 103–1		Hyp. 12–4 Pig. 12–6	Pig. 63–2	Hyp. 74–4	Pig. 68–4	Pig. 103–2

[a] Total Fe as FeO.

32 other analyses can be obtained by writing to the authors.

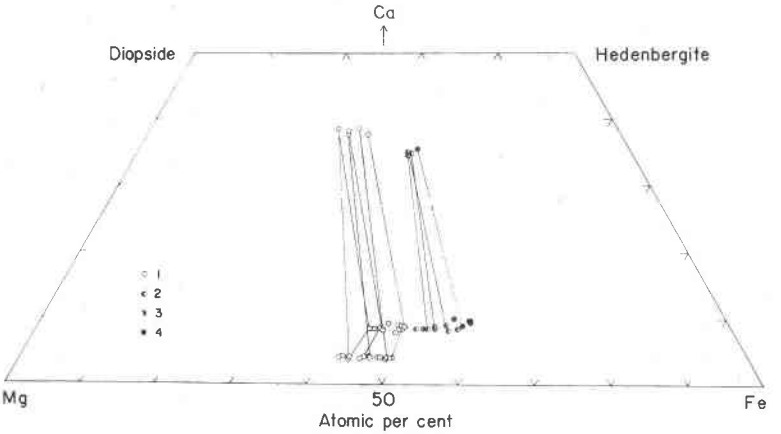

FIG. 1. Ca–Mg–Fe plot of the analyzed pyroxenes. Symbols: open circles (1), phenocryst pyroxenes; half solid circles (2), rim of phenocryst pyroxenes; half solid circles (3), microphenocryst pyroxene; solid circles (4), groundmass pyroxenes. Solid lines are selected tie lines connecting those pyroxenes which occur as contiguous crystals.

(Figs. 1 and 2). The partition coefficient for Mg–Fe has been determined between contacting hypersthene and pigeonite, hypersthene and augite, and pigeonite and augite (Table 2). It is to be noted that the partition coefficient (K_D) is calculated on the assumption that total iron is ferrous. Because ferric iron may be higher in augite than in Ca-poor pyroxenes, the K_D for $Mg\text{-}Fe^{2+}$ parition between augite and Ca-poor pyroxenes

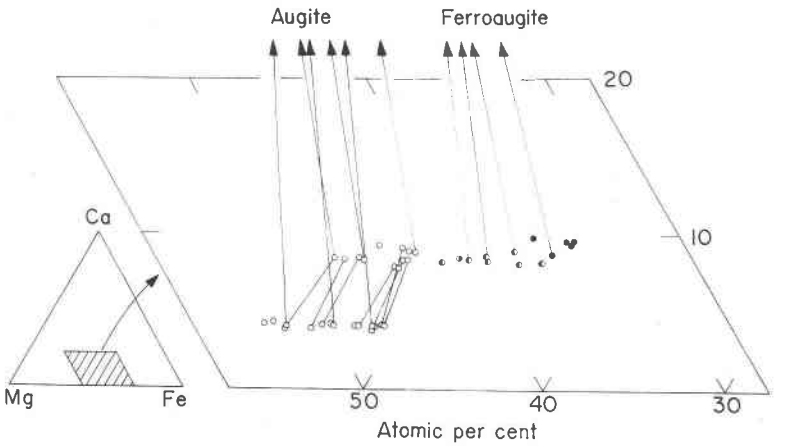

FIG. 2. Ca–Mg–Fe plot of the analyzed Ca-poor pyroxenes. Symbols as in Fig. 1. Solid lines are tie lines connecting those pyroxenes which occur as contiguous crystals.

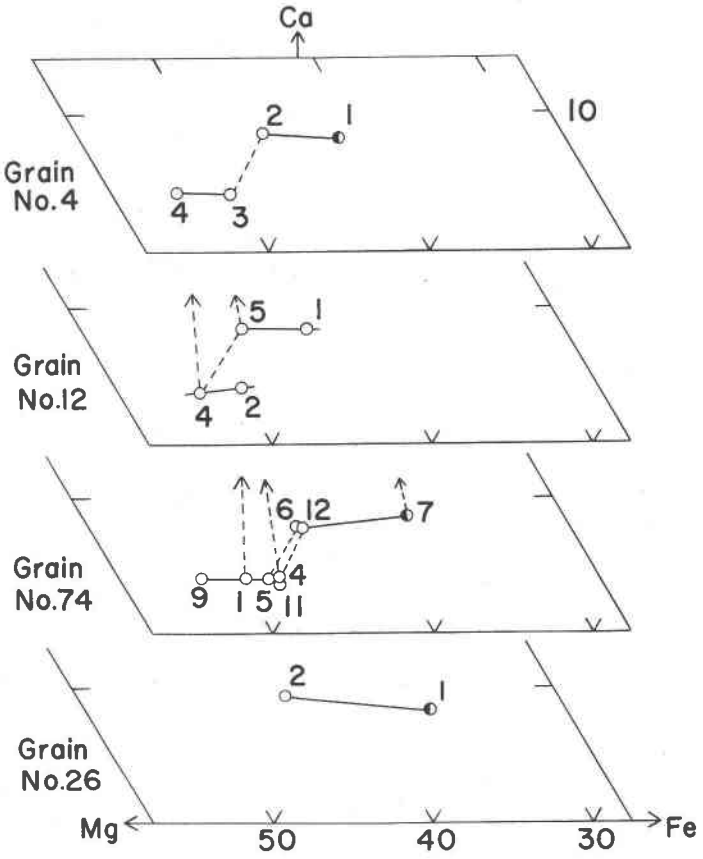

FIG. 3. Portions of the Ca–Mg–Fe diagram showing compositional zonings within single pyroxene grains No. 4, 12, 74 and 26. Numbers in the diagrams are those of point of analysis. Solid lines indicate continuous zoning, and dashed lines indicate tie lines connecting different pyroxenes which occur as contiguous crystals.

may be smaller than the values given in Table 2. The partition coefficients for Ca-poor pyroxene and Ca-rich pyroxene are, therefore, considered to be comparable with those of the Skaergaard intrusion (0.73 in an average by Atkins, 1969). However, those for the pairs of contiguous pigeonite and augite, both of which occur as rims to the pigeonite phenocrysts, and for a pair of groundmass augite and pigeonite, are relatively large. Since the compositional change is steep near the margin of pigeonite phenocrysts, and since augite has crystallized at the margin of pigeonite (Fig. 6B), augite may have crystallized at a slightly later stage of fractionation than pigeonite and may not have been in equilib-

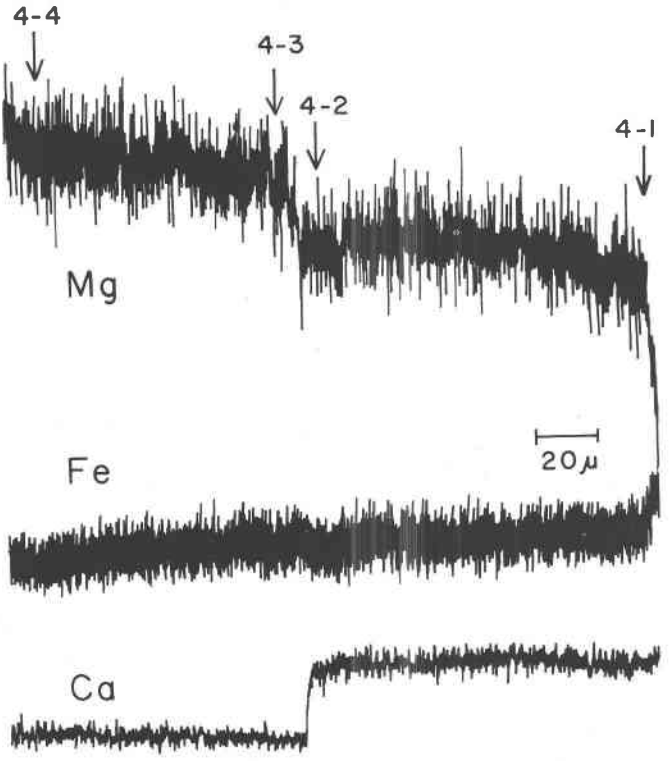

FIG. 4. Scanning of hypersthene-pigeonite composite phenocryst (grain No. 14), showing compositional zoning and points of analysis.

rium with the analyzed pigeonite part. The partition coefficients for hypersthene and pigeonite pairs are nearly the same as those for the groundmass hypersthene and pigeonite pairs of the Hakone andesite given by Nakamura and Kushiro (1970) (*i.e.* $K_D = 1.09$ on average). The compositional gaps between augite and hypersthene phenocrysts and between augite and pigeonite of both phenocryst and groundmass generations are considerably wide (*i.e.*, 35–26 mole % Ca). They are wider than those of the Hakone andesite pyroxenes (Nakamura and Kushiro, 1970) and the Skaergaard intrusion pyroxenes (Brown, 1957). It should be emphasized that no subcalcic augite has been found to bridge the gap between augite and pigeonite of either phenocryst or groundmass generation. The compositional boundary between the Ca-rich and Ca-poor pyroxenes is always sharp (Fig. 6).

The Al–Ti relations of the analyzed pyroxenes are shown in Figure 7. Hypersthene, pigeonite and augite fall in separate areas of this figure.

TABLE 2. PARTITION COEFFICIENT OF MG–FE BETWEEN CONTACTING PYROXENES

	Hypersthene		Pigeonite		K_D[a]
	Point of analysis	X_{Mg}	Point of analysis	X_{Mg}	
Phenocryst	4– 3	0.524	4– 2	0.502	1.09
	12– 4	0.547	12– 6	0.518	1.13
	22– 4	0.531	22– 3	0.512	1.08
	69– 2	0.488	69– 1	0.473	1.06
	69– 4	0.489	69– 5	0.476	1.05
	69– 9	0.494	69–10	0.475	1.08
	74– 5	0.502	74– 6	0.481	1.09
	74–11	0.495	74–12	0.480	1.06
	average				1.08

	Hypersthene		Augite		K_D[b]
	Point of analysis	X_{Mg}	Point of analysis	X_{Mg}	
Phenocryst	12– 4	0.547	12– 5	0.595	0.82
	74– 1	0.517	74– 2	0.572	0.80
	74– 4	0.495	74– 3	0.550	0.80
	average				0.81

	Pigeonite		Augite		K_D[c]
	Point of analysis	X_{Mg}	Point of analysis	X_{Mg}	
Phenocryst core	12– 6	0.518	12– 5	0.595	0.73
	22– 2	0.499	22– 1	0.574	0.74
	63– 2	0.468	63– 3	0.531	0.78
	average				0.75
Groundmass and rim of phenocryst	68– 2	0.435	68– 1	0.451	0.94
	68– 4	0.424	68– 3	0.443	0.93
	74– 7	0.408	74– 8	0.451	0.84
	103– 2	0.385	103– 1	0.432	0.82
	average				0.88

[a] $K_D = \dfrac{X_{Mg}^{Hyp}}{1 - X_{Mg}^{Hyp}} \cdot \dfrac{1 - X_{Mg}^{Pig}}{X_{Mg}^{Pig}}$, where $X_{Mg} = \dfrac{Mg}{Mg + Fe}$

[b] $K_D = \dfrac{X_{Mg}^{Hyp}}{1 - X_{Mg}^{Hyp}} \cdot \dfrac{1 - X_{Mg}^{Aug}}{X_{Mg}^{Aug}}$

[c] $K_D = \dfrac{X_{Mg}^{Pig}}{1 - X_{Mg}^{Pig}} \cdot \dfrac{1 - X_{Mg}^{Aug}}{X_{Mg}^{Aug}}$

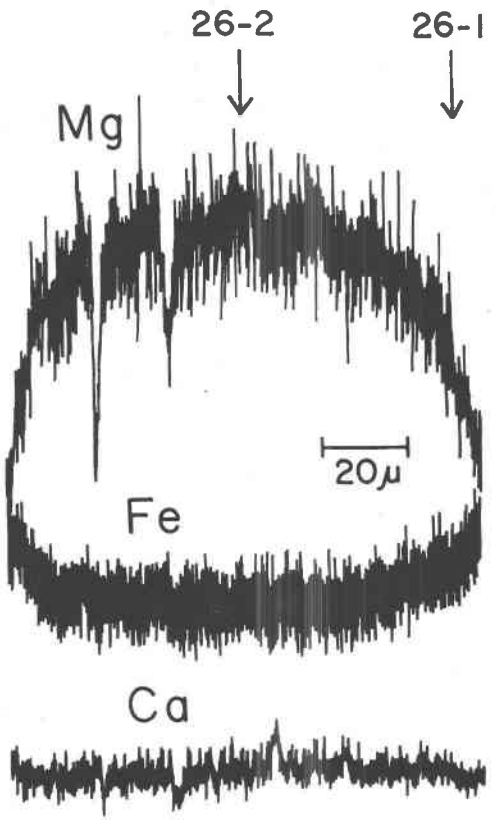

FIG. 5. Scanning of pigeonite-ferropigeonite phenocryst (grain No. 26) by Ca, Mg and Fe Kα, showing a symmetrical continuous zoning. Number indicates point of analysis. Sharp drop of X-ray intensity is due to rough surface of the sample.

It is noteworthy that hypersthene is always more Al and Ti-rich than the contacting pigeonite and that Al and Ti decrease regularly from core to margin of hypersthene phenocrysts, whereas Al decreases and Ti increases from core to margin of pigeonite phenocrysts. The Si–Al relations of the analyzed pyroxenes are shown in Figure 8. Most of the analyzed pyroxenes plot above the line $Si+Al=2$, indicating that some Al is in the octahedral site.

The Fe–Mn relations are shown in Figure 9. Augite and pigeonite have a nearly constant Mn/Fe ratio, whereas hypersthene has a lower Mn/Fe ratio than the clinopyroxenes. These relations were confirmed by the analysis of contiguous orthopyroxene and clinopyroxenes. The same relations have been observed in the Hakone andesite. Na content

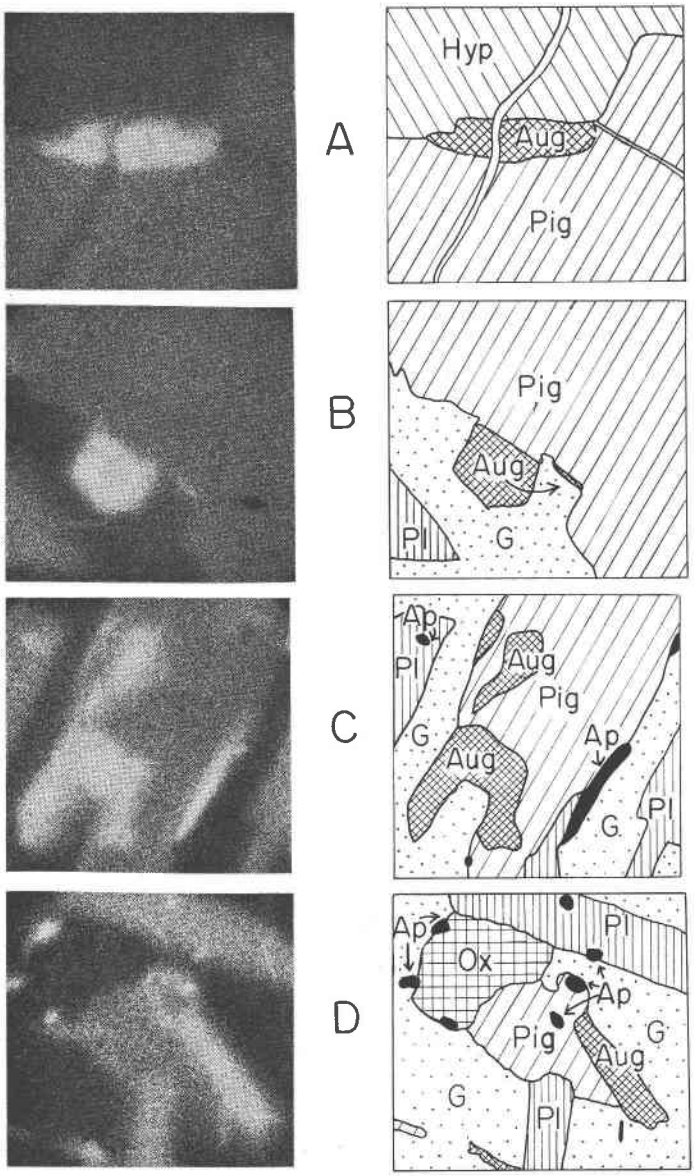

FIG. 6. Beam scanning photographs of pyroxenes by Ca Kα. A: augite inclusion at the boundary of hypersthene and pigeonite (grain No. 12, analyses 12-4, 5 and 6 in Table 1). B: ferroaugite at the margin of pigeonite-ferropigeonite phenocryst (grain No. 68, analyses 68-3 and 4). C: groundmass composite grain of ferropigeonite and ferroaugite (grain No. 103, analyses 103-1 and 2). D: ditto (grain No. 108, analysis 108). Abbreviations: Aug, augite and ferroaugite; Ap, apatite; G, glass; Hyp, hypersthene and ferrohypersthene; Ox, Fe-Ti oxide mineral; Pig, pigeonite and ferropigeonite; Pl, plagioclase. The length of one side of each photograph corresponds to 40 μm.

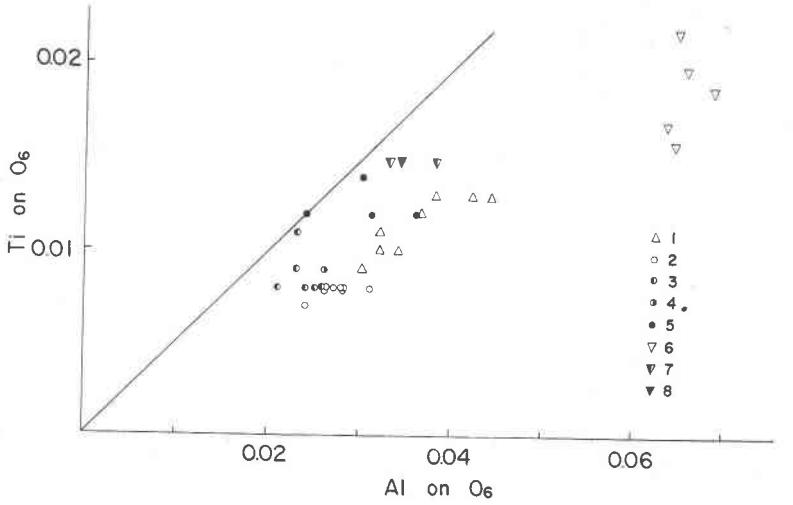

FIG. 7. Ti–Al relations of the analyzed pyroxenes. Symbols: 1, phenocryst hypersthene-ferrohypersthene; 2, phenocryst pigeonite-ferropigeonite; 3, ferropigeonite rim of phenocryst; 4, micro-phenocryst ferropigeonite; 5, groundmass ferropigeonite; 6, phenocryst augite; 7, ferroaugite rim of phenocryst; 8, groundmass ferroaugite. Numbers for Ti and Al are based on 6 oxygens.

is higher in augite (0.24 weight percent Na_2O on average), intermediate in pigeonite (0.07%) and lowest in hypersthene (0.04%). The Na content is most probably related to the Fe^{3+} content (*i.e.* acmite component).

Plagioclase has been analyzed partially by microprobe. The compositional range of phenocryst plagioclase is $An_{70}Ab_{30}$-$An_{45}Ab_{55}$. Groundmass plagioclase has a composition near $An_{45}Ab_{55}$, which is the same as that of a thin rim to phenocryst plagioclase. The zoning of phenocryst plagioclase is strong near the margin as compared with that in the core.

The glass has been analyzed (Table 3) with a wide electron beam (20 μm). The glass includes unidentified minute crystals (width less than 1μm). The analysis represents the bulk composition of the glass and these minute crystals. A poor total for the analysis as at least partly due to the presence of water in the glass. The bulk chemical composition of this andesite (p. 3) shows 3.6 weight percent H_2O+. Since anhydrous crystals occupy a considerable part ($\sim$33 percent) of this rock, the glass should contain about 5.4 weight percent H_2O. The composition of the glass recalculated to a water-free oxide percentage is rhyolitic, although some normative corundum is calculated.

DISCUSSION

The compositional and textural relations of the coexisting hypersthene, pigeonite and augite indicate that the phenocryst pyroxene

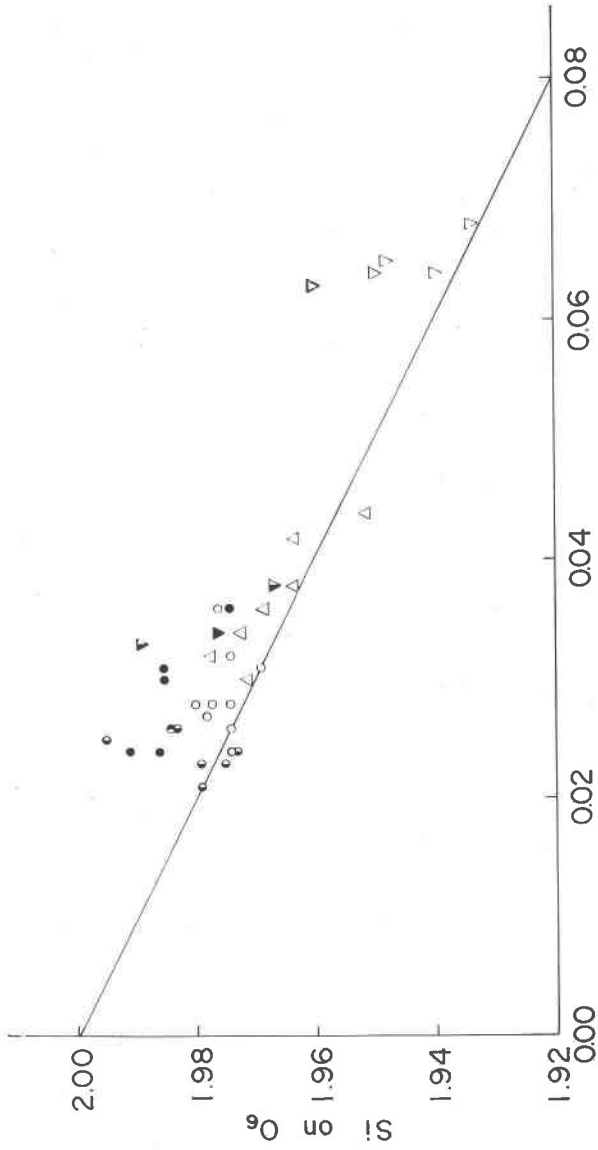

Fig. 8. Si–Al relations of the analyzed pyroxenes. Symbols as in Fig. 7. Numbers for Si and Al are based on 6 oxygens.

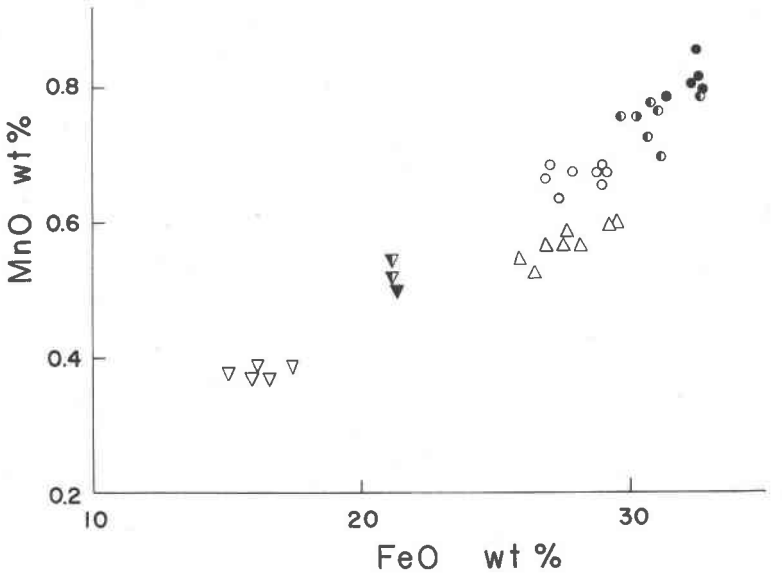

FIG. 9. MnO–FeO relations of the analyzed pyroxenes. Symbols as in Fig. 7.

assemblage in the Weiselberg pigeonite andesite varies from hypersthene-augite of relatively low Fe/Mg ratio through hypersthene-augite-pigeonite of varying Fe/Mg ratio to augite-pigeonite of relatively high Fe/Mg ratio. The groundmass pyroxene assemblage is augite

TABLE 3. COMPOSITION AND NORM OF GLASS IN THE GROUNDMASS OF WEISELBERG ANDESITE

			Norm (wt. %)	
SiO_2	71.7	2[b]		
Al_2O_3	11.5	1	Q	38.5
TiO_2	0.48	1	or	12.6
FeO[a]	2.10	4	ab	40.1
MnO	0.04	—	an	2.98
MgO	0.09	—	en	0.25
CaO	0.56	2	fs	3.38
Na_2O	4.40	1	il	0.99
K_2O	1.99	2	C	1.19
Total[c]	92.9		Total	100.0

[a] Total iron as FeO.

[b] $\sigma/\sqrt{\bar{N}}$ values by Boyd (1967), where σ is the standard deviation and $\bar{N}$ the arithmetic mean of the X-ray counts.

[c] Poor total is partly due to the presence of water (see text).

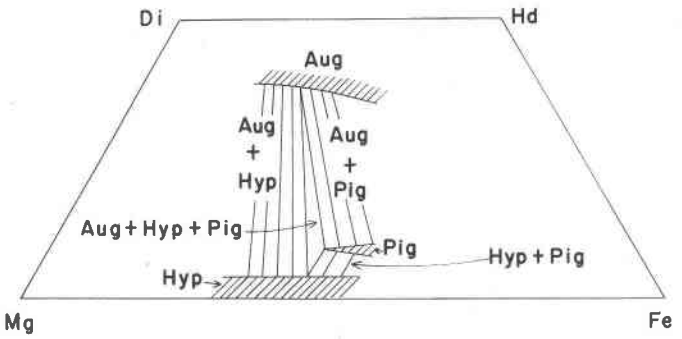

FIG. 10. Schematic isothermal section at a subsolidus temperature of the pyroxene quadrilateral diopside (Di); enstatite (En); ferrosilite (Fs); hedenbergite (Hd). Abbreviations as in Fig. 6.

and pigeonite of relatively high Fe/Mg ratio. As shown in Figures 1 and 2, at least two different three-phase triangles for the hypersthene-pigeonite-augite assemblage can be drawn. Because a three-phase triangle is fixed at one set of temperature and pressure conditions in the $CaSiO_3$–$MgSiO_3$–$FeSiO_3$ system, the present results clearly indicate that the conditions of equilibration of the pyroxenes varied during the crystallization history. Pressure is unlikely to have changed much during the crystallization and, therefore, temperature change would be a major cause for the shift of the three-phase triangle. Several different three-phase triangles can be drawn for a wide range of Fe/Mg ratio from the analyses of coexisting phenocryst orthopyroxene, pigeonite and augite of various Japanese volcanic rocks (Kuno and Inoue, 1949; Kuno, 1950; Aoki, 1960; Oba, 1960; Isshiki, 1963) and a Beaver Bay diabase (Muir, 1954).

A part of the subsolidus isothermal section of the system diopside-enstatite-ferrosilite-hedenbergite is shown in Figure 10. A similar isothermal section in the iron-rich portion has been drawn by Bonnischsen (1969) on the basis of the metamorphosed Biwabik Iron Formation. In the Weiselberg andesite, as well as in several other rocks, the pyroxene assemblage varies from augite-hypersthene through augite-hypersthene-pigeonite to augite-pigeonite. It is to be expected that the three-pyroxene region shifts toward iron-rich compositions with lowering temperature. This is illustrated in Figure 11a, which is a temperature-composition diagram along the join $Ca_{10}Mg_{90}(A)$–$Ca_{10}Fe_{90}(B)$ in the Ca–Mg–Fe diagram. As shown in the figure, pigeonite is considered to have a stability field at a higher temperature than augite+hypersthene of the same Fe/Mg ratio, and the temperature of the three-pyroxene region decreases with increase in Fe/Mg ratio. This three-pyroxene region is

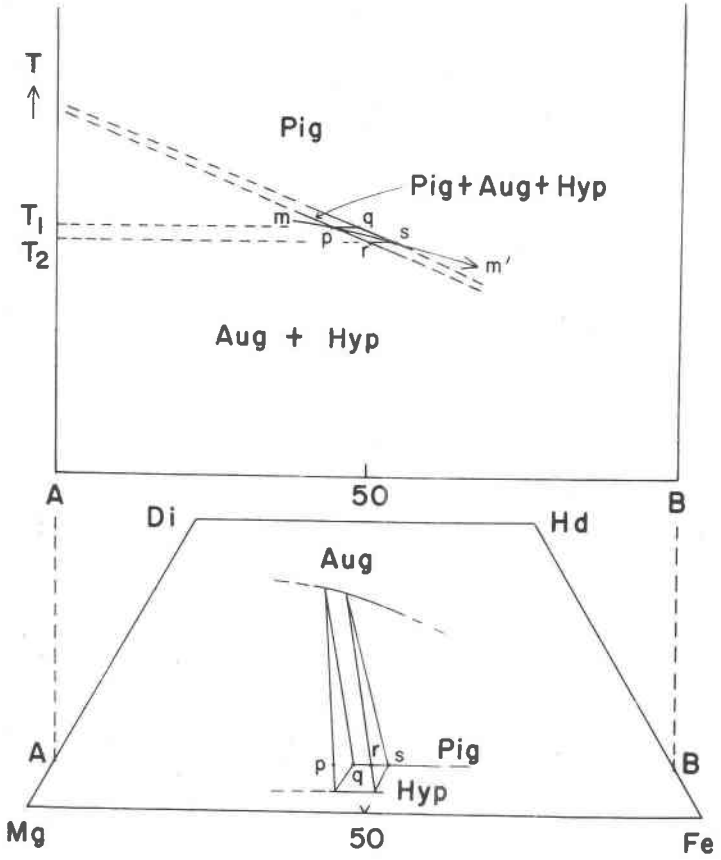

FIG. 11. Schematic diagram showing the crystallization of pyroxenes in Weiselberg andesite. Two three-phase triangles are based on the analyses of Weiselberg pyroxenes. $m \rightarrow m'$ indicates temperature change of magma during the crystallization of the Weiselberg andesite. Note that the intervals p-q and r-s are not the 'inversion interval' but the maximum widths along the join A–B of three phase triangle hypersthene-pigeonite-augite at temperatures T_1 and T_2, respectively.

different in temperature from the orthopyroxene-clinopyroxene inversion interval of the Ca-free join $MgSiO_3$–$FeSiO_3$ determined by Bowen and Schairer (1935) and involves the additional phase of augite. The variation of assemblage and the compositional relations of the Weiselberg pyroxenes are explained well by this diagram. The pyroxene assemblage just before pigeonite crystallization was hypersthene+augite, the bulk composition and the temperature of which are represented by m in Figure 11a. As the temperature decreased and the composition of crystallized pyroxenes became richer in Fe, pigeonite of composition q began to crystallize at T_1. Three pyroxenes continued to coexist

stably until the temperature fell to T_2. At temperature T_2, hypersthene ceased to crystallize from the magma. It should be noted that this crystallization course is for the bulk composition of the crystallized pyroxenes lying on the join A–B. If the bulk pyroxene composition is not on the join A–B, hypersthene ceases to crystallize at temperatures higher than T_2 and at an Fe/Mg ratio lower than s. At temperatures below T_2, augite (ferroaugite) and pigeonite (ferropigeonite) would crystallize side by side from the magma. In the Skaergaard intrusion (Brown, 1957), the bulk composition hypersthene+augite would have entered three-pyroxene region at a temperature higher than in the Weiselberg andesite because augite, hypersthene and pigeonite in the three-pyroxene region are more magnesian in the Skaergaard intrusion. This interpretation is similar to that initially proposed by Hess (1941); however, as mentioned before, the present interpretation is based on the idea that pigeonite is essentially a Ca-bearing mineral and its stability field relative to that of augite+hypersthene is not dependent on the stability field of clinopyroxene relative to that of orthopyroxene in the Ca-free join $MgSiO_3$–$FeSiO_3$.

The replacement of hypersthene by pigeonite during the crystallization is a result of reaction hypersthene+liquid$\rightleftharpoons$pigeonite. The liquid involved in this reaction must be more Ca and Fe-rich than these three pyroxenes. Pigeonite occurs as phenocrysts in many volcanic rocks, suggesting that pigeonite is most likely a primary liquidus phase in natural magmas; however, its initial structure could be different from that observed at room temperature. Yoder, Tilley, and Schairer (1963) suggested that protohypersthene might be a high temperature form of pigeonite, although the other possibility that pigeonite is a quenched stable phase was also considered. Pigeonite crystallizing as a primary liquidus phase might be a clinopyroxene with C-centered monoclinic lattice as has been suggested by Morimoto and Tokonami (1969). Such transformation in pigeonite does not affect the present argument insofar as the composition of the high-temperature clinopyroxene would be the same as that of pigeonite. The present argument also does not depend on whether there is a continuous solid solution between pigeonite and high-temperature clinopyroxene on the $MgSiO_3$–$FeSiO_3$ join ($C2/c$) shown by Smyth (1969) or there is a miscibility gap between pigeonite and $MgSiO_3$–$FeSiO_3$ pyroxene as suggested by Kushiro (1969). It is emphasized that clinopyroxene of pigeonite composition (regardless of its initial structure) has a high temperature stability field relative to hypersthene+augite and *not* to hypersthene only.

ACKNOWLEDGMENTS

We are grateful to Dr. H. S. Yoder, Jr., Professor Emeritus Seitaro Tsuboi and member-

of the Geological Institute, the University of Tokyo for their discussion and encouragement.

References

Aoki, K. (1960) Early stage basalts from the Nasu volcanic zone. *J. Jap. Ass. Mineral. Petrologists Econ. Geol.* **45,** 54–65. [in Japanese]

Atkins, F. B. (1969) Pyroxenes of the Bushveld Intrusion, South Africa. *J. Petrology,* **10,** 222–249.

Bonnichsen, B. (1969) Metamorphic pyroxenes and amphiboles in the Biwabik iron formation, Dunka river area, Minnesota. *Mineral. Soc. Amer. Spec. Pap.* **2,** 217–239.

Bowen, N. L., and J. F. Schairer (1935) The system MgO–FeO–SiO_2. *Amer. J. Sci.* **29,** 151–217.

Boyd, F. R. (1967) Quantitative electron-probe analysis of pyroxenes. *Carnegie Inst. Wash. Year Book,* **66,** 327–334.

Brown, G. M. (1957) Pyroxenes from the early and middle stages of fractionation of the Skaergaard instrusion east Greenland. *Mineral. Mag.* **31,** 511–543.

Hess, H. H. (1941) Pyroxenes of common mafic magmas. Part 1 and part 2. *Amer. Mineral.* **26,** 515–535; 573–594.

Isshiki, N. (1963) Petrology of Hachijo-jima Volcano Group, Seven Izu Islands, Japan. *J. Fac. Sci. Univ. Tokyo, Sec. 2,* **15,** 91–134.

Kuno, H. (1947) Occurrence of porphyritic pigeonite in 'weiselbergite' from Weiselberg, Germany. *Proc. Jap. Acad.* **23,** 111–113.

——— (1950) Petrology of Hakone Volcano and the adjacent areas, Japan. *Geol. Soc. Amer. Bull.* **61,** 957–1020.

——— (1955) Ion substitution in the diopside-ferropigeonite series of clinopyroxenes. *Amer. Mineral.* **40,** 70–93.

——— (1966) Review of pyroxene relations in terrestrial rocks in the light of recent experimental works. *Mineral. J.* **5,** 21–43.

———, and T. Inoue (1949) On porphyritic pigeonite in andesite from Okubo-yama, Minami-Aizu, Hukusima Prefecture. *Proc. Jap. Acad.* **25,** 121–132.

Kushiro, I. (1969) The system forsterite-diopside-silica with and without water at high pressures. *Amer. J. Sci.* **267-A,** 269–294.

———, and Y. Nakamura (1970) Petrology of some lunar crystalline rocks. *Geochim. Cosmochim. Acta, Supplement I (Lunar Volume),* 607–626

Muir, I. D. (1954) Crystallization of pyroxenes in an iron-rich diabase from Minnesota. *Mineral. Mag.* **30,** 376–388.

Nakamura, Y. and I. Kushiro (1970) Compositional relations of coexisting orthopyroxene, pigeonite and augite in a tholeiitic andesite from Hakone volcano. *Contrib. Mineral. Petrology,* **26,** 265–275.

Oba, Y. (1960) On the phenocrystic pigeonite in a somma lava of Usu volcano, Hokkaido. *J. Jap. Ass. Mineral. Petrologists Econ. Geol.* **46,** 172–177.

Rosenbusch, H. (1887) *Mikroskopisch Physiographie der Massigen Gestein. 2 ed,* Stuttgart, p. 501.

Smyth, J. R. (1969) Orthopyroxene-high-low clinopyroxene inversions. *Earth Planet. Sci. Lett.* **6,** 406–407.

Tröger, E. (1935) Quantitative Daten einiger magmatischer Gestein. *Tschermak's Mineral. Petrogr. Mitt.* **46,** 153–173.

Yoder, H. S., Jr., C. E. Tilley and J. F. Schairer (1963) Pyroxene quadrilateral. *Carnegie Inst. Wash. Year Book,* **62,** 84–95.

Manuscript received, June 8, 1970; accepted for publication, July 21, 1970.